Strain Rate Effects on Head-on Quenching of Laminar Premixed Methane-air flames

Yujuan Luo[1] · Christina Strassacker[2] · Xu Wen[1] · Zhen Sun[1] · Ulrich Maas[2] · Christian Hasse[1]

Abstract

Head-on quenching is a canonical configuration for flame-wall interaction. In the present study, the transient process of a laminar premixed flame impinging on a wall is investigated for different strain rates, while previous studies with detailed chemistry and transport focused only on unstrained conditions. Increasing strain rate leads to a reduction in the normalized quenching distance, and an increase in the normalized wall heat flux, both are considered as global flame quantities. Looking more into the local microstructure of the quenching process, CO formation and oxidation near the wall are shifted to higher temperatures under higher strain rates. Further, the local flame structure and the thermochemical state are affected by differential diffusion driven by differences in species' gradients and diffusivities. Quenching leads to increased species' gradients and consequently differential diffusion is amplified near the wall compared to propagating flames. However, this effect is suppressed for increasing strain rates, which is explained in more detail by a source term analysis of the transport equation for the differential diffusion parameter Z_{HC}. Results for the global quantities and the local flame structure show that the impact of the strain rate weakens for higher wall temperatures. Finally, the analyses of the thermo-chemical quantities in the composition space shows that H_2 can be a good parameter to characterize the strain rate both for propagating and quenching flamelet.

Keywords Head-on quenching (HOQ) · Strain rate · Differential diffusion · Stretched flames

✉ Yujuan Luo
  luo@stfs.tu-darmstadt.de

1 Simulation of Reactive Thermo-Fluid Systems, TU Darmstadt, Otto-Berndt-Straße 2, 64287 Darmstadt, Germany

2 Institute of Technical Thermodynamics, Karlsruhe Institute of Technology, Engelbert-Arnold-Straße 4, 76131 Karlsruhe, Germany

1 Introduction

Flame-wall interaction is a common phenomenon in confined combustion chambers such as internal combustion engines and gas turbines (Dreizler and Böhm 2015). The presence of the wall significantly affects the flame structure, and causes the flame to quench, which leads to lower combustion efficiency and increased pollutant formation. In addition, high wall heat fluxes can become a major safety issue.

Head-on quenching (HOQ) and side wall quenching (SWQ) are two generic quenching configurations. Comparatively, looking at global flame characteristics, HOQ results in a smaller quenching distance and higher wall heat flux than SWQ as the flame front impinges vertically on the wall (Boust et al. 2007). This makes HOQ a well-defined limiting case suitable for parametric investigations and consequently this work focuses on the HOQ scenario.

The flow field in HOQ can be either laminar or turbulent. Turbulence adds another level of complexity to HOQ since turbulence-chemistry interaction and turbulence-wall interaction must be considered in addition to flame-wall interaction (Poinsot et al. 1993; Bruneaux et al. 1996; Zhao et al. 2018; Lai and Chakraborty 2016; Lai et al. 2018). Only flame-wall interaction is involved in laminar HOQ, which makes it a suitable configuration to gain deeper insight into flame-wall interaction. Also, results from laminar HOQ can support the development of turbulent near-wall combustion models. Besides, simple configuration such as the laminar HOQ are suitable for complementary experimental and numerical studies. Laminar HOQ has been extensively studied in previous studies (Boust et al. 2007; Hocks et al. 1981; Ezekoye et al. 1992; Popp and Baum 1997; Hasse et al. 2000; Dabireau et al. 2003; Chauvy et al. 2010; Strassacker et al. 2018; Jiang et al. 2019; Bellenoue et al. 2003; Foucher et al. 2003; Sotton et al. 2005; Mann et al. 2014).

Laminar HOQ is always a transient process where the premixed flame propagates through either initially stagnant mixtures (unstrained) or convective flows (strained). In this work, we use the term strain solely to characterize the underlying flow field, which then results in a stretched flame. Until now, both experimental (Bellenoue et al. 2003; Foucher et al. 2003; Sotton et al. 2005) and numerical (Boust et al. 2007; Poinsot et al. 1993; Lai and Chakraborty 2016; Lai et al. 2018; Hocks et al. 1981; Ezekoye et al. 1992; Popp and Baum 1997; Hasse et al. 2000; Dabireau et al. 2003; Chauvy et al. 2010; Jiang et al. 2019) studies related to laminar flame have almost exclusively focused on stagnant and therefore unstrained conditions. Specifically, the configuration of a freely propagating flame impinging on the wall has been studied for different fuel types, wall temperatures, and pressures in numerical simulations (Boust et al. 2007; Poinsot et al. 1993; Lai and Chakraborty 2016; Lai et al. 2018; Hocks et al. 1981; Ezekoye et al. 1992; Popp and Baum 1997; Hasse et al. 2000; Dabireau et al. 2003; Chauvy et al. 2010; Jiang et al. 2019). By contrast, there have been only a very limited number of investigations into laminar strained flow conditions (Bruneaux et al. 1996; Strassacker et al. 2018; Mann et al. 2014), and to the best of our knowledge no numerical studies with detailed chemistry and diffusive transport that conduct a systematic variation of strain rate exist in the literature. Bruneaux et al. (1996) simulated wall quenching of laminar flames in a stagnation line flow using one-step chemistry and simplified diffusion modeling. Mann et al. (2014) conducted the first measurements of the temperature and CO concentration under strained flow conditions. Strassacker et al. (2018) performed corresponding numerical simulations of this configuration using the Reaction-Diffusion-Manifold (REDIM) approach (Bykov and Maas 2007), however the underlying tabulated manifold was generated using gradient information from

an unstrained HOQ configuration. The results showed reasonable agreement with the (strained) experimental data.

Previous numerical studies (Ganter et al. 2017; Strassacker et al. 2019) reported that differential diffusion is an important phenomenon during flame-wall interaction. For example, Ganter et al. (2017) reported that when using mixture-averaged diffusion, the simulation results show better agreement with the SWQ experimental data compared to the unity Lewis number assumption. Strassacker et al. (2019) performed an unstrained HOQ simulation, and also confirmed that detailed transport models lead to improved predictions compared to simplified transport models. However, the relevance for varying and especially high-strain conditions is still unknown.

Approaches using a tabulated manifold, e.g. REDIM- or flamelet-based, are widely-used for numerical simulations. While the flamelet model has been extended to consider strain rate effects in premixed flames (Knudsen et al. 2013; Oijen and Goey 2002; Trisjono et al. 2016; Peters 2000), it has not yet been investigated for near-wall combustion. To consider strain, an additional parameter is introduced. Different parameters including the H radical (Knudsen et al. 2013), CO (Oijen and Goey 2002), H_2 (Trisjono et al. 2016) and the dissipation rate (Peters 2000) have been used to represent the strain rate effects. Consequently, we will extend these investigations to near-wall combustion by evaluating the suitability of these parameters to characterize the strain rate effects.

Based on the above literature review, the scope of the current study is to investigate transient HOQ of laminar premixed flames in a counterflow configuration for varying strain rates. The validity of the numerical approach is first evaluated through comparisons with experimental results. Then, strain rate effects on the global quenching quantities (quenching distance, wall heat flux) considering varying wall temperatures are studied. Next, the micro-structure of the quenching flame is analyzed through the local thermo-chemical state in CO/T phase space and near-wall differential diffusion. Finally, guidance is offered for developing a flamelet model for near-wall combustion.

1.1 Governing equations

The strained premixed HOQ problem can be described by the 1D unsteady opposed-flow equations for mass, axial momentum, radial momentum, energy and species (Im 2000), which are based on the conservation equations in cylindrical coordinate, with the assumption that the distributions of axial velocity, scaled radial velocity, temperature and species mass fractions are similar near the centerline, so that they are functions of time and the axial coordinate only: $u = u(t,x)$, $V = v/r = V(t,x)$, $T = T(t,x)$, $Y_k = Y_k(t,x)$.

Based on the assumption that $V = v/r = V(t,x)$, mass continuity equation can be written as:

$$\frac{\partial \rho}{\partial t} + \frac{\partial}{\partial x}(\rho u) + \frac{1}{r}\frac{\partial}{\partial r}(\rho v r) = \frac{\partial \rho}{\partial t} + \frac{\partial}{\partial x}(\rho u) + 2\rho V = 0 \tag{1}$$

The equation of state:

$$\rho = \frac{PW}{RT} \tag{2}$$

where the total thermodynamic pressure P is the sum of a reference pressure p_0 and a varying pressure p, which is the dependent variable.

By differentiating Eq. (2), following relation can be obtained:

$$\frac{\partial \rho}{\partial t} = \frac{\rho}{P}\frac{\partial p}{\partial t} - \frac{\rho}{T}\frac{\partial T}{\partial t} - \rho W \sum_k \frac{1}{W_k}\frac{\partial Y_k}{\partial t} \tag{3}$$

Substituting Eq. (3) into the Eq. (1), the mass continuity equation can be finally expressed as:

$$\frac{\rho}{P}\frac{\partial p}{\partial t} - \frac{\rho}{T}\frac{\partial T}{\partial t} - \rho W \sum_k \frac{1}{W_k}\frac{\partial Y_k}{\partial t} + \frac{\partial}{\partial x}(\rho u) + 2\rho V = 0 \tag{4}$$

Similarly, the axial momentum and radial momentum equations can also be simplified using the assumption $u = u(t,x)$ and $v/r = V(t,x)$, which finally read:

$$\rho\frac{\partial u}{\partial t} + \rho u\frac{\partial u}{\partial x} + \frac{\partial p}{\partial x} - 2\mu\frac{\partial V}{\partial x} - \frac{4}{3}\frac{\partial}{\partial x}\left(\mu\frac{\partial u}{\partial x}\right) + \frac{4}{3}\frac{\partial}{\partial x}(\mu V) = 0 \tag{5}$$

$$\rho\frac{\partial V}{\partial t} + \rho u\frac{\partial V}{\partial x} + \rho V^2 - \frac{\partial}{\partial x}\left(\mu\frac{\partial V}{\partial x}\right) + \Lambda = 0$$
$$\Lambda \equiv \frac{1}{r}\frac{\partial p}{\partial r} = \Lambda(t) \tag{6}$$

The energy equation can be simplified with the assumption that $T = T(t,x)$, which finally leads to the equation:

$$\rho c_p\frac{\partial T}{\partial t} + \rho c_p u\frac{\partial T}{\partial x} - \frac{\partial}{\partial x}\left(\lambda\frac{\partial T}{\partial x}\right) - \frac{\partial p}{\partial t} - u\frac{\partial p}{\partial x} + \rho\left(\sum_k c_p Y_k V_k\right)\frac{\partial T}{\partial x} + \sum_k \omega_k W_k h_k = 0 \tag{7}$$

For species equation, assuming $Y_k = Y_k(t,x)$, it can be written as:

$$\rho\frac{\partial Y_k}{\partial t} + \rho u\frac{\partial Y_k}{\partial x} + \frac{\partial}{\partial x}(\rho Y_k V_k) - \omega_k W_k = 0 \qquad (k = 1, ..., n_s) \tag{8}$$

In Eqs. (1)–(8), t stands for time. x is the axial direction and r is the radial direction. ρ denotes density. T is the temperature. Y_k is the mass fraction of the k-th species. W is the mixture-averaged molecular weight while W_k stands for the molecular weight of the k-th species. u represents the axial velocity, while v is the radial velocity, and the scaled radial velocity is denoted as V. Λ is the eigenvalue of the system, which is time-dependent. P stands for the total pressure, which consists of a reference pressure p_0 and a varying pressure p. μ is the dynamic viscosity. c_p is the specific heat. λ stands for heat conductivity. ω_k denotes the molar reaction rate of the k-th species. h_k is the enthalpy of formation of the k-th species. V_k is the species' diffusion velocity, which is considered by both mixture-averaged model and equal diffusivity model (unity Lewis number) in the present study. n_s is the total number of species. R stands for the universal gas constant.

The above system of DAEs (differential–algebraic equations) is solved with the in-house solver ULF (Zschutschke et al. 2017). A second-order central differencing scheme is used for spatial discretization. Time integration is implemented with an implicit, variable-order, variable-step method based on the Gear multi-value method (Buzzi Ferraris and Manca 1998) which is suitable for stiff DAE systems. All simulations start from a steady solution as initial condition. GRI-Mech 3.0 (Smith et al. 1999) is used for the combustion chemistry.

2 Numerical implementation

2.1 Computational domain

The configuration studied is schematically shown in Fig. 1. A stoichiometric homogeneous methane/air mixture is injected from a nozzle, and propagates towards the wall. The bulk flow velocity at the nozzle exit is U_0. Consistent with the experimental setup (Mann et al. 2014), the premixed flow is ignited downstream by a spark, establishing a strained premixed flame propagating towards the wall.

The computational domain extends from the nozzle exit to the wall, which is set to be 10 mm. The coordinate system is defined as shown in Fig. 1 such that x is in axial direction, being zero at the wall surface and positive in the upstream direction, while r is in the radial direction. The domain is initially filled with a stoichiometric homogeneous methane/air mixture at 1 atm. To avoid preheating, the unburnt gas and the wall temperature are set to be equal. The computational domain is discretized by 1200 grid points with local refinement near the wall, resulting a mesh resolution of 5 μm in the near-wall region.

2.2 Boundary conditions

At the inlet, the axial velocity u is set to be constant, which equals to the value at the nozzle exit U_0. The scaled radial velocity V is set to zero. The temperature T and species mass fractions Y_k are set to be the same of the unburnt gas.

The axial velocity u is set to zero at the wall, while zero-gradient boundary condition is applied for scaled radial velocity V. The wall temperature T_w is set to be constant. Consistently with a previous study (Jiang et al. 2019), the wall is assumed to be inert and consequently a zero-diffusion flux boundary condition $\rho V_k Y_k = 0$ is employed for all species.

Similarly to (Escudié et al. 1999), the strain rate K is defined as the mean axial velocity gradient near the wall, which can be varied by adjusting the inlet velocity. Since the

Fig. 1 Schematic of the system configuration for the transient HOQ process
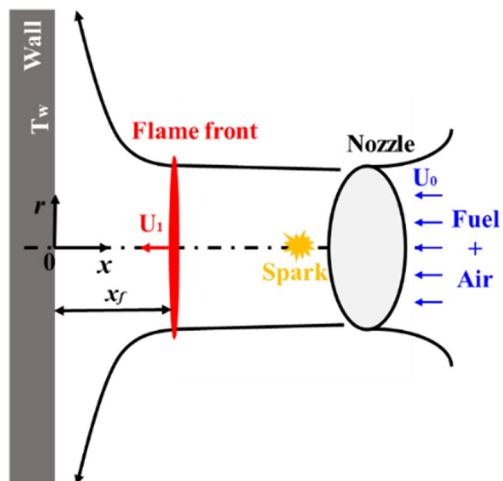
value of K changes during the transient flame propagation, it is calculated based on the initial state of the flow field prior to ignition. It is found that the wall temperature and the diffusion model have only little impact on the exact value of the strain rate. In the present study, four different strain rates of 600 s^{-1}, 1200 s^{-1}, 1800 s^{-1}, and 2400 s^{-1} are investigated for two distinctively different wall temperatures relevant for confined combustion (Bruneaux et al. 1996) (T_w = 300 K, 600 K), as summarized in Table 1. The wall distance where the axial flow velocity $|u|$ equals the unstretched adiabatic laminar burning velocity s_L^0 (T_w = 300 K, mixture-averaged model) is also included for reference.

2.3 Dimensionless parameters

For comparing the current results with the literature and to quantify the effect of strain rate, dimensionless parameters previously used in quenching studies are employed.

The distance between the flame front and the wall (x_f) is often expressed in its dimensionless form as a Peclet number (Popp and Baum 1997)

$$Pe = \frac{x_f}{\delta},\tag{9}$$

where δ is the thickness of a laminar adiabatic unstretched flame $\delta = \lambda_u/(\rho_u c_p s_L^0)$, where λ_u and ρ_u are the thermal conductivity and density of the unburnt gas, respectively. c_p is the specific heat capacity per unit mass. The flame front position corresponds to the location of the maximum heat release rate, which is consistent with previous studies (Dabireau et al. 2003; Palulli et al. 2019).

The instant of quenching (t_Q) is defined as the time instant of the maximum wall heat flux $q_{wall,max} = (\lambda \partial T/\partial x|_{wall})_{max}$, which is consistent with other numerical studies (Strassacker et al. 2019). The dimensionless form of wall heat flux is $Q = q_{wall}/[\rho s_L^0 c_p(T_{ad} - T_u)]$, where T_{ad} is the adiabatic flame temperature and T_u is the temperature of the unburnt gas. The flame-wall distance at quenching instant is defined as quenching distance $x_{f,Q} = x_f (t = t_Q)$, with the corresponding Peclet number $Pe_Q = x_{f,Q}/\delta$. Based on the definitions above, the dimensionless time τ is expressed as

$$\tau = \frac{t - t_Q}{\delta/s_L^0}.\tag{10}$$

Besides, the wall distance x is normalized as

$$D_w = \frac{x}{\delta}.\tag{11}$$

Table 1 Summary of investigated conditions

Strain rate K (s^{-1})	Wall distance (m) where $|u| = s_L^0$	Wall temperature T_w (K)
600	6.62e–4	300, 600
1200	3.25e–4	300, 600
1800	2.12e–4	300, 600
2400	1.61e–4	300, 600

3 Results and discussion

In this section, the available experimental data is firstly used to validate the numerical solver. Using the validated solver, the effects of strain rates and wall temperature are investigated in a systematic manner next.

3.1 Validation and comparison to experiments

The simulation results are first compared to the experimental data reported in (Mann et al. 2014), which includes the temperature and CO concentration measured through two-photon laser-induced fluorescence (LIF) and nanosecond coherent anti-Stokes Raman spectroscopy of nitrogen (CARS), respectively. Unless specifically indicated, otherwise, all simulations use a mixture-averaged model for the diffusion velocities.

Figure 2 shows the CO mole fraction X_{CO} over the temperature T for different positions, such plots in phase space were originally presented in (Mann et al. 2014) and are also used here for comparison. Also indicated are the two branches for CO formation and oxidation, which are characteristic for premixed flames, more details can be found in (Kosaka et al. 2018). Experimental results are shown as scatter data and a corresponding mean; the variance from the fluctuations is shown as an error bar. At different locations, the trends in the variation of CO against T are similar. At the beginning, the CO level increases along with the temperature (CO formation branch). After the peak value is reached, CO decreases due to oxidation. The CO level drops with initially increasing and later decreasing temperature depending on the wall distance. However, non-negligible differences between the simulations and experiments can be observed for positions near the wall, which is consistent with the findings in (Strassacker et al. 2018). This can be seen mostly for the oxidation branch, e.g. Fig. 2b, c, but also for the formation branch in
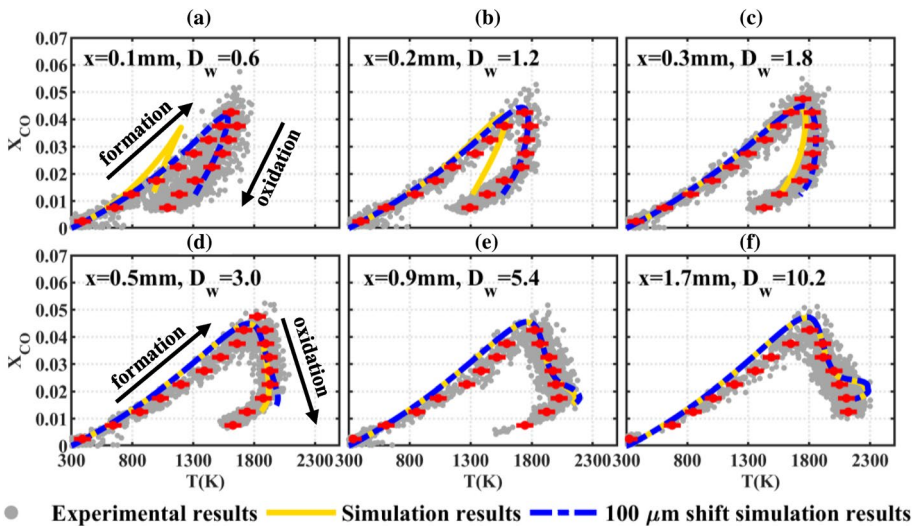

Fig. 2 CO mole fraction over temperature for different positions until 0.5 ms after quenching (numerical results are obtained using mixture-averaged diffusion model). The error bar is obtained according to the experimental fluctuations (Kosaka et al. 2018)

the very near-wall position, as in Fig. 2a. These differences can be partially attributed to experimental uncertainties for wall distance determination. The wall in the experiments is convex which is part of a sphere with a radius of $R_{wall} = 300$ mm. The maximum value of the uncertainty is estimated to be 100 μm (Dreizler A 2019). Thus, we additionally show simulation results shifted by 100 μm, which show very good agreement with experiments for all wall distances. It is evident that in the very near-wall region, the shift has a significant effect on the CO-T variation, see e.g. at $x = 0.1$ mm. However, such effects become almost insignificant for locations far away from the wall, e.g. for $x = 1.7$ mm, because the wall influence on the flame structure decreases with increasing distance from the wall. Further away from the wall, the wall influence can be neglected and both CO formation and oxidation branches correspond to a freely-propagating flame. For these regions, discrepancies between numerical results and experimental data, especially in the formation branch, may be attributed to the chemistry mechanism and the influence of initial ignition which is generated by placing an artificial time-decaying energy source near the inlet, with the latter effect becoming negligible in the near-wall region.

Figure 3a shows the evolution of the temperature as a function of the dimensionless time τ and normalized wall distance D_w. It can be clearly seen that as the flame propagates towards the wall, the near-wall temperature increases. After quenching, the temperature first decreases in the near-wall region, and then spreads towards regions away from the wall. The corresponding evolution of the CO mole fraction is shown in Fig. 3b. It can be seen that CO does not vanish during or even after quenching, and it remains high within the quenching distance, which is consistent with the experimental data as reported above.

In summary, the comparison between the numerical and experimental results show favorable agreement. Furthermore, our numerical results for this reference case are comparable to previously reported works, and differences to experimental results can at least partially be attributed to uncertainties in the determination of the wall position. In the following section, the influences of strain on the quenching process both in terms of global quantities and local thermochemical structures are investigated.

3.2 Global quenching parameters and local thermo-chemical state

As indicated above the quenching distance is the flame-wall distance at time instant of quenching. It is a key parameter quantifying the thickness of the unburnt layer.
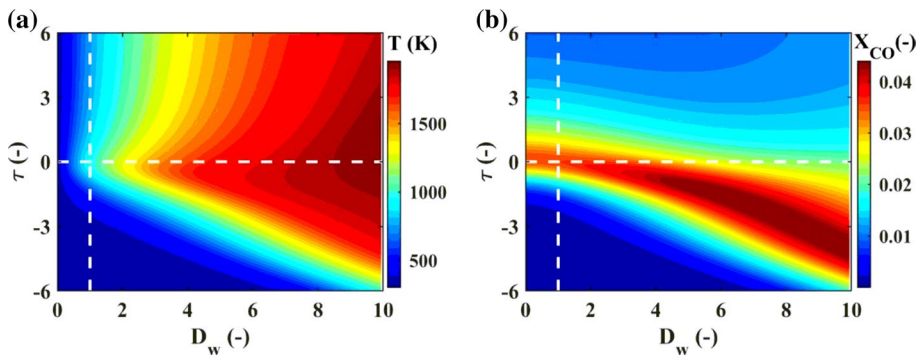

Fig. 3 D_w-τ plots of **a** temperature and **b** CO mole fraction for experimental setup. The horizontal line represents the normalized quenching distance. The vertical line represents the quenching instant

Dimensionless quenching distances (Pe_Q) for different strain rates and different wall temperatures, see Table 1, are plotted in Fig. 4a, where the subscript Q denotes the instant of quenching. In addition to the mixture-averaged diffusion model, results obtained with the unity Lewis number assumption are shown for comparison. Overall, Pe_Q decreases with an increasing strain rate, which is a direct consequence of the underlying flow pushing the flame towards the wall. However, for a higher wall temperature, these strain rate effects on Pe_Q become less pronounced. For example, for $T_w = 300$ K, Pe_Q decreases from 2.66 to 1.96 for a strain variation of 600 s^{-1} to 2400 s^{-1} using a mixture-averaged diffusion model. By contrast, for $T_w = 600$ K and the same diffusion model, the maximum difference in Pe_Q is only 0.01. Comparing Pe_Q for different wall temperatures for the same strain rate, it can be seen that Pe_Q decreases as the wall temperature increases. This specific trend is consistent with previous findings in the literature for unstrained HOQ (Norden 1965). The gap becomes narrower as the strain rate increases. Finally, for both $T_w = 300$ K and $T_w = 600$ K, the unity Lewis number assumption leads to an underestimation of Pe_Q compared to the mixture-averaged model, which are mainly due to the differences in absolute values of quenching distance x_f and laminar burning velocity s_L^0. This confirms that a unity Lewis number is not suitable for laminar HOQ of methane-air flames.

The non-dimensional wall heat flux is another key quantity in flame-wall interaction. Following the definition above and consistent with previous works, Q_Q denotes the normalized wall heat flux at the quenching instant. Figure 4b shows the normalized quenching wall heat flux for different strain rates and different wall temperatures. Overall, a higher strain rate results in a larger wall heat flux. This is closely related to the variation in the Pe_Q number. It is interesting to note that the variation in Q_Q is more distinct for smaller strain rates. At higher wall temperatures, the normalized wall heat flux almost stays constant at a value of 0.66 for varying strain rates, which is consistent with the unstrained value reported in (Popp and Baum 1997). The difference between the results calculated using unity Lewis number assumption and mixture-averaged diffusion becomes significant for lower wall temperatures and higher strain rates, which is mainly caused by the differences in laminar burning velocity s_L^0, the adiabatic flame temperature T_{ad}, as well as the near-wall temperature gradient. This finding again confirms that the unity Lewis number assumption is unsuitable here and therefore it will not be considered further in the remainder of the study.
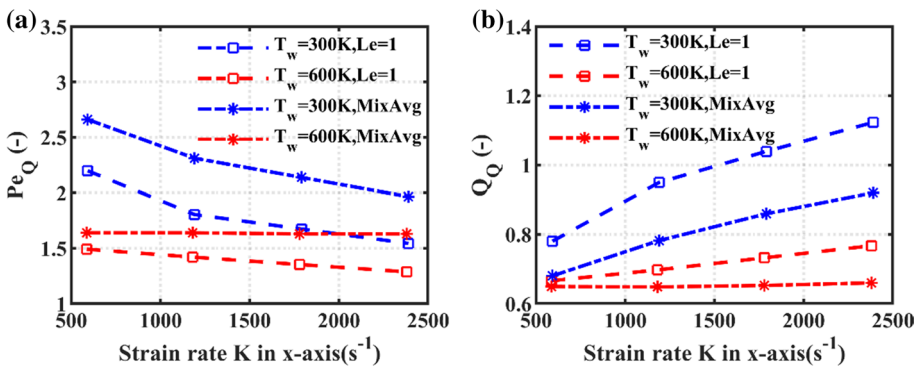

Fig. 4 Normalized global quantities: **a** quenching distances, **b** quenching wall heat flux

After the discussion of the global quantities, we now turn our attention to the local thermochemical state in vicinity of the wall and how it is affected by strain. Figure 5 presents CO-T variations under different strain rates for different positions ($D_w = 1, 2, 3$), and two wall temperatures of 300 K and 600 K are shown. The positions are chosen to be within the quenching region, see the discussion on the Peclet number above. The results are recorded until $\tau = 0.5$. It is seen that CO profiles vary strongly at the different positions and for the two wall temperatures. Closer to the wall, both CO formation and oxidation happen under lower temperature conditions.

From these results it is evident that strain rate effects on the thermo-chemical state are especially obvious for $T_w = 300$ K. At a higher strain rate, both the formation and the oxidation branch move to a higher temperature. Close to the wall, the strain rate has a larger influence on the formation branch than on the oxidation branch. Further away from the wall, the strain rate effect on CO-T decreases and remains only important for the oxidation branch. This can be confirmed by looking specifically at $D_w = 3$, the formation branches for different strain rates almost overlap.

Summarizing the analyses of quenching distances, wall heat flux and CO-T variation, the strain rate has a significant effect at lower wall temperatures. Contrarily, the effect almost diminishes at higher wall temperatures and this applies both for the global quantities and the local microstructure. Therefore, in the subsequent discussion, we focus on cases with $T_w = 300$ K to investigate the impact of strain on differential diffusion.

3.3 Strain rate effects on differential diffusion

As a first step, we quantify the impact of differential diffusion on the quenching process for the case $T_w = 300$ K and $K = 600$ s^{-1}. Then, we analyze the influence of varying strain rates.
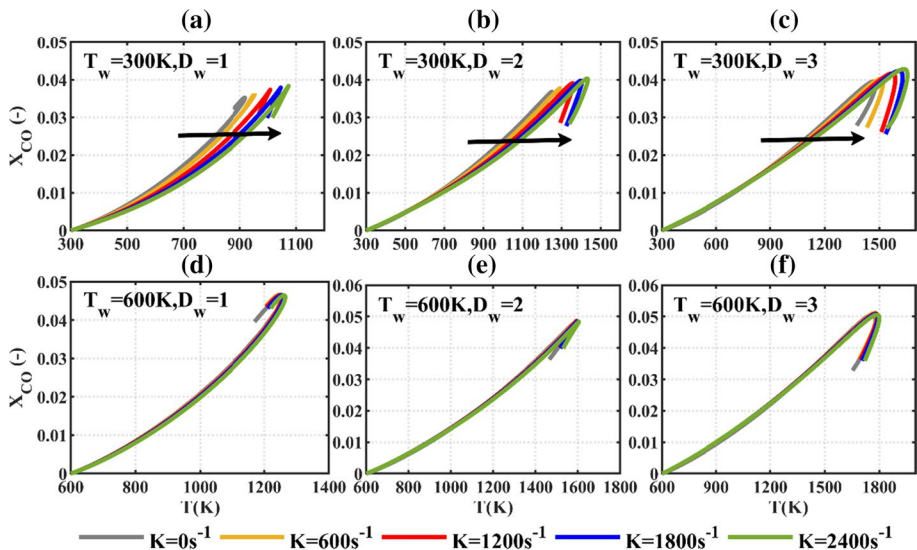

Fig. 5 CO-T plot for different positions until 0.5 dimensionless time after quenching

For this analysis, we use the differential diffusion parameter Z_{HC} to quantify the degree of differential diffusion

$$Z_{HC} = F_H - F_C, \tag{12}$$

where $F_H = (Y_H - Y_{H,1})/(Y_{H,2} - Y_{H,1})$ and $F_C = (Y_C - Y_{C,1})/(Y_{C,2} - Y_{C,1})$ (Barlow et al. 2000). Y stands for the mass fraction of the respective element (H or C), and subscripts 1 and 2 refer to pure fuel (here methane) and air (i.e. $Y_{C,2} = Y_{H,2} = 0$), respectively. Larger absolute values of Z_{HC} indicate stronger differential diffusion. Note that the main focus of the present study is the variation of Z_{HC}, rather than the Z_{HC} value itself, which might strongly differ for other fuels.

Figure 6 shows the Z_{HC} profile as a function of the normalized wall distance for different times. Symbols on the lower abscissa denote the flame front position at the respective time (indicated by the color). At different times, the minimum (largest absolute) value of Z_{HC} always occurs ahead of the position of maximum heat release towards the preheat zone, i.e. between the reaction zone and the wall. As the flame approaches the wall, the minimum of Z_{HC} moves towards the wall and differential diffusion within the quenching distance becomes more pronounced. The smallest value of Z_{HC} is found just prior to quenching, and it exceeds the value of the propagating flame by a factor of up to 2 in terms of absolute numbers. This is consistent with the findings above concerning the change of the local thermochemical state during quenching.

For the subsequent analysis of differential diffusion during HOQ, the balance equation for differential diffusion parameter Z_{HC} is considered. Using Eq. (12), the total derivative can be expressed as

$$\rho \frac{DZ_{HC}}{Dt} = \frac{1}{Y_{H,2} - Y_{H,1}} \rho \frac{DY_H}{Dt} - \frac{1}{Y_{C,2} - Y_{C,1}} \rho \frac{DY_C}{Dt}. \tag{13}$$

The balance equations for elemental mass fractions are

$$\rho \frac{DY_H}{Dt} = -\nabla \cdot \left(\sum_{k=1}^{n_s} \frac{a_{kH} W_H}{W_k} \rho Y_k V_k \right), \tag{14}$$

Fig. 6 Differential diffusion parameter profile at different times for $T_w = 300$ K, $K = 600$ s^{-1}
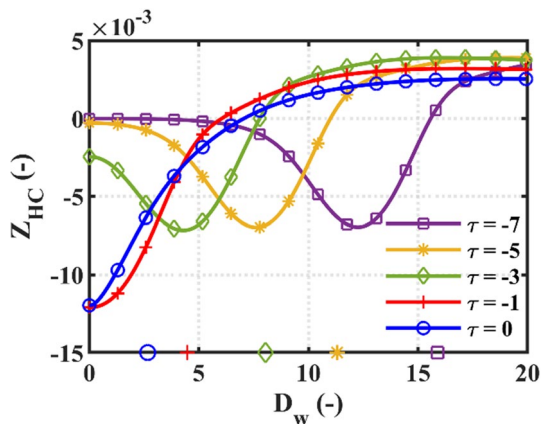
$$\rho \frac{DY_C}{Dt} = -\nabla \cdot \left(\sum_{k=1}^{n_s} \frac{a_{kC} W_C}{W_k} \rho Y_k V_k \right), \tag{15}$$

where W stands for the molecular weight. V_k is the diffusion velocity of species k. a_{kH} is the number of atoms of element H in a molecule of species k, a_{kC} is the number of atoms of element C in a molecule of species k.

For a unity Lewis number assumption, the diffusion term for Z_{HC} can be expressed as $-\nabla \cdot (\rho D \nabla Z_{HC})$, where D is the diffusion coefficient of Z_{HC} and all species. Combining Eqs. (13)–(15), the governing equation for Z_{HC} can be rearranged as

$$\rho \frac{DZ_{HC}}{Dt} - \nabla \cdot (\rho D \nabla Z_{HC})$$
$$= \frac{-\nabla \cdot \left(\sum_{k=1}^{n_s} \frac{a_{kH} W_H}{W_k} \rho V_k Y_k \right)}{Y_{H,2} - Y_{H,1}} - \frac{-\nabla \cdot \left(\sum_{k=1}^{ns} \frac{a_{kC} W_C}{W_k} \rho V_k Y_k \right)}{Y_{C,2} - Y_{C,1}} - \nabla \cdot (\rho D \nabla Z_{HC}) \tag{16}$$

The right-hand side of Eq. (16) represents the deviation from a scalar with unity Lewis number and therefore it is a direct measure for the importance of differential diffusion.

Figure 7 presents the evolution of the source term at different times up to quenching for $K = 600$ s^{-1} (a) and $K = 1800$ s^{-1} (b), respectively. For reference, the Z_{HC} profiles are also plotted. Prior to quenching, the shape of the source term remains similar for all times with negative values just ahead of the flame front and positive values around the reaction zone, which is the expected profile for propagating flames without wall influence. As long as the flame is far away from the wall, the source term near the wall is zero, see e.g. $\tau = -5$ for both strain rates. As the flame approaches the wall, the source term in the near wall region begins to decrease until the instant of quenching, when the positions of minimum source term and minimum Z_{HC} (see also Fig. 6) are both located at the wall. Compared to the propagating flames, both the source term and Z_{HC} decrease to smaller values (larger absolute values).

Both maximum and minimum Z_{HC} source terms are amplified by higher strain rate for the propagating flames, resulting in a small difference in minimum and maximum Z_{HC} value. However, when the flame interacts with wall, the minimum Z_{HC} value for $K = 600$ s^{-1} at $\tau = 0$ is significantly smaller compared to $K = 1800$ s^{-1} meaning that strain
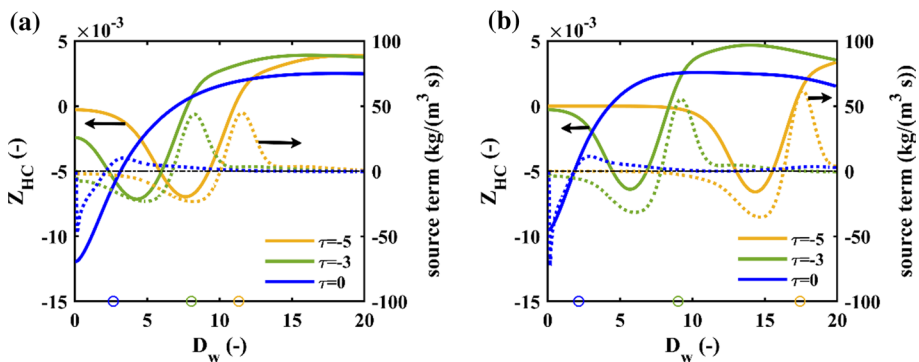

Fig. 7 Source term (dotted line) and Z_{HC} (solid line) profiles at different times for **a** $K = 600$ s^{-1}, and **b** $K = 1800$ s^{-1}

dampens differential diffusion near the wall during quenching. In contrast, the source term decreases with increasing strain rate, which reflects the larger magnitude of species' gradients near the wall.

This is further analyzed in Fig. 8, where the minimum Z_{HC} value (Z_{HCmin}) is plotted as a function of time, as is the location $D_w | Z_{HC} = Z_{HCmin}$. When the flame is far away from the wall, the minimum Z_{HC} value is almost constant during propagation, confirming the rather small influence of strain as discussed above. However, when the flame enters the near-wall region (see discussion on Peclet number above), a minimum of Z_{HCmin} occurs right before quenching with a slight delay (τ values closer to zero) for higher strain rates. Further, the higher the strain rate, the later starts the departure from the propagating flame and this is also reflected in the trajectory of $D_w | Z_{HC} = Z_{HCmin}$. The location of the minimum Z_{HC} value occurs later in the quenching region for higher strain rate. In fact, this explains why Z_{HCmin} does increase with strain. Although the source term is amplified by strain, the smaller residence time in the quenching layer leads to dampening of differential diffusion.

3.4 Guidance to near-wall flamelet modeling

In strained premixed flamelet modelling, an additional parameter is introduced to characterize strain rate effects (Knudsen et al. 2013; Oijen and Goey 2002; Trijsono et al. 2016; Peters 2000). It should be sensitive to strain rate, and it is crucial that there is no overlap between different profiles, so that a unique value can be found for a table look-up. This section mainly focuses on finding a suitable strain parameter for near-wall flamelet modeling.

In Fig. 9, three different scalars previously used for strain parameterization, Y_H, Y_{CO} and Y_{H_2}, are plotted against progress variable. Here, the progress variable (PV) is defined as $PV = Y_{CO_2} + Y_{H_2O} + Y_{CO} + Y_{H_2}$ (Knudsen et al. 2013). Two time instants are chosen: $\tau = -1$ represents the time before quenching, while the other time $\tau = 0$ corresponds to the quenching instant. As shown in Fig. 8a, before quenching, both Y_H and Y_{H_2} show a strong sensitivity to the strain rate, while Y_{CO} varies only little. It is hard to distinguish Y_{CO} between different strain rates, so Y_{CO} is not a suitable choice for the time before quenching. At the instant of quenching, Y_H does not show a monotonic variation with the strain rate as before. Different profiles overlap, so a lack of uniqueness will be encountered for tabulation. At the quenching instant, Y_{H_2} is a suitable strain rate parameter. Although the variation trend is in

Fig. 8 Minimum Z_{HC}-value (solid line) within $D_w = 0$–20 and its location $D_w | Z_{HC} = Z_{HCmin}$ (dashed line) plotted over time
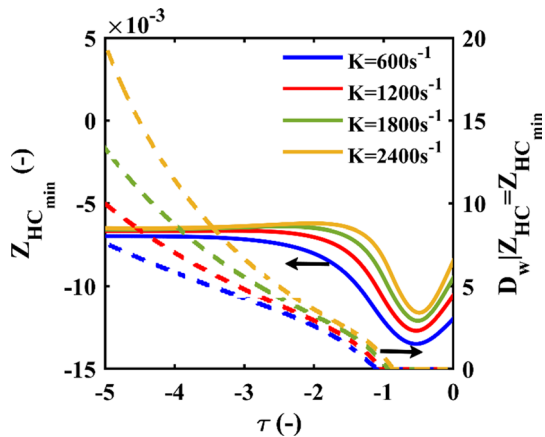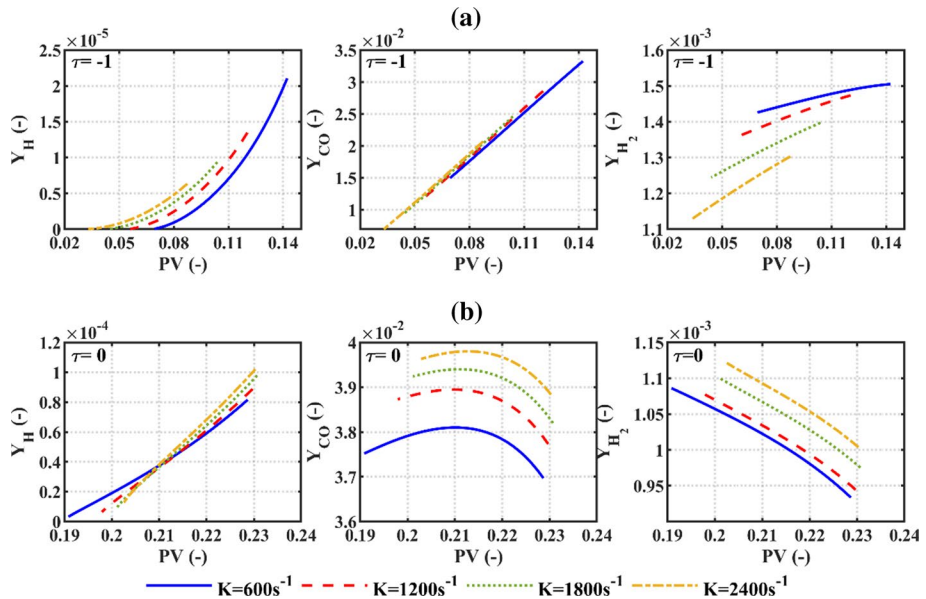
Fig. 9 Different species plotted against progress variable for different strain rates prior and at quenching

opposition to the time before quenching, the monotonicity over the strain rate is retained. Based on the above analysis for the cases studied, H_2 is suitable to parameterize strain rate for the near-wall flamelet modelling.

4 Conclusions

The present numerical study investigated the transient head-on quenching (HOQ) of stretched premixed laminar methane-air flames using detailed chemistry and transport. While previous studies in the literature focused on unstrained conditions, this work is the first study of laminar HOQ systematically varying the strain rate for different wall temperatures. After validating the numerical approach against experimental data, this work specifically focused on four aspects.

1. The impact of strain rate on the global quantities: The normalized quenching distance expressed as Peclet number Pe_Q decreases with increasing strain rate, while the normalized wall heat flux increases. This can be directly attributed to the underlying flow field supporting flame propagation towards the wall. Modelling species' diffusion with a unity Lewis number is not sufficient and this applies for low and high strain rates. The impact of strain is generally higher for low wall temperatures while it is negligible at 600 K.
2. The impact of strain on the near-wall microstructure: the local flame structure is analyzed with CO-T profiles in phase space at various wall distances. Strain influences both the CO formation and oxidation branches. Close to the wall, strain affects mostly CO formation while further away, the oxidation branch is shifted to higher temperatures

with increasing strain. The impact of strain is generally more pronounced for lower wall temperatures and it is negligible at 600 K, which is consistent with the findings for the global quantities above.

3. The impact of strain on near-wall differential diffusion: the effect of non-equal diffusivities is quantified by the parameter Z_{HC}. Differential diffusion is substantially enhanced in the quenching layer compared to propagating flames. While strain has little influence on the minimum/maximum Z_{HC} values in the propagating flame, higher strain rates do suppress the increase of differential diffusion in the near-wall quenching layer. This aspect is further quantified by studying the source term in the transport equation for Z_{HC}. While the source term is amplified by strain, the main effect is the reduction of residence time in the near-wall region for higher strain rates.

4. Parameterization of strain rate for manifold-based tabulation approaches: It was shown in previous works that the effect of strain on the structure of a stretched premixed flame can be parameterized by a reactive scalar. This finding is extended here for quenching flames. Results show that the H_2 is well-suited for parameterizing strain rate for propagation and quenching, while other scalars previously used for propagating flames are not applicable during quenching. While the parameterization should only be used for the conditions tested, our findings can be considered a good starting point when looking at other conditions.

Compliance with ethical standards

Conflict of interest The authors declare that they have no conflict of interest.

References

Barlow, R.S., Fiechtner, G.J., Carter, C.D., Chen, J.Y.: Experiments on the scalar structure of turbulent CO/H2/N2 jet flames. Combust. Flame **120**(4), 549–569 (2000). https://doi.org/10.1016/S0010-2180(99)00126-1

Bellenoue, M., Kageyama, T., Labuda, S.A., Sotton, J.: Direct measurement of laminar flame quenching distance in a closed vessel. Exp. Therm. Fluid Sci. **27**(3), 323–331 (2003)

Boust, B., Sotton, J., Labuda, S.A., Bellenoue, M.: A thermal formulation for single-wall quenching of transient laminar flames. Combust. Flame **149**(3), 286–294 (2007). https://doi.org/10.1016/j.combustflame.2006.12.019

Bruneaux, G., Akselvoll, K., Poinsot, T., Ferziger, J.H.: Flame-wall interaction simulation in a turbulent channel flow. Combust. Flame **107**(1), 27–44 (1996). https://doi.org/10.1016/0010-2180(95)00263-4

Buzzi Ferraris, G., Manca, D.: BzzOde: a new C++ class for the solution of stiff and non-stiff ordinary differential equation systems. Comput. chem. eng **22**(11), 1595–1621 (1998)

Bykov, V., Maas, U.: The extension of the ILDM concept to reaction–diffusion manifolds. Combust. Theor. Model. **11**(6), 839–862 (2007). https://doi.org/10.1080/13647830701242531

Chauvy, M., Delhom, B., Reveillon, J., Demoulin, F.-X.: Flame/wall interactions: laminar study of unburnt HC formation. Flow Turb. Combust. **84**(3), 369–396 (2010). https://doi.org/10.1007/s10494-009-9245-8

Dabireau, F., Cuenot, B., Vermorel, O., Poinsot, T.: Interaction of flames of $H_2 + O_2$ with inert walls. Combust. Flame **135**(1), 123–133 (2003). https://doi.org/10.1016/S0010-2180(03)00154-8

Dreizler, A.: Personal communication (2019).

Dreizler, A., Böhm, B.: Advanced laser diagnostics for an improved understanding of premixed flame-wall interactions. Proc. Combust. Inst. **35**(1), 37–64 (2015). https://doi.org/10.1016/j.proci.2014.08.014

Escudié, D., Haddar, E., Brun, M.: Influence of strain rate on a premixed turbulent flame stabilized in a stagnating flow. Exp. Fluids **27**(6), 533–541 (1999). https://doi.org/10.1007/s003480050377

Ezekoye, O., Greif, R., Sawyer, R.F.: Increased surface temperature effects on wall heat transfer during unsteady flame quenching. In: Symposium (International) on Combustion, 1992/01/01/ 1992, vol. 1, pp. 1465–1472

Foucher, F., Burnel, S., Mounaïm-Rousselle, C., Boukhalfa, M., Renou, B., Trinité, M.: Flame wall interaction: effect of stretch. Exp Therm Fluid Sci **27**(4), 431–437 (2003). https://doi.org/10.1016/S0894-1777(02)00255-8

Ganter, S., Heinrich, A., Meier, T., Kuenne, G., Jainski, C., Rißmann, M., Dreizler, A., Janicka, J.: Numerical analysis of laminar methane–air side-wall-quenching. Combust. Flame **186**, 299–310 (2017). https://doi.org/10.1016/j.combustflame.2017.08.017

Hasse, C., Bollig, M., Peters, N., Dwyer, H.A.: Quenching of laminar iso-octane flames at cold walls. Combust. Flame **122**(1), 117–129 (2000). https://doi.org/10.1016/S0010-2180(00)00107-3

Hocks, W., Peters, N., Adomeit, G.: Flame quenching in front of a cold wall under two-step kinetics. Combust. Flame **41**, 157–170 (1981). https://doi.org/10.1016/0010-2180(81)90049-3

Im, H.G.: Numerical studies of transient opposed-flow flames using adaptive time integration. KSME Int. J. **14**(1), 103–112 (2000). https://doi.org/10.1007/bf03184776

Jiang, B., Gordon, R.L., Talei, M.: Head-on quenching of laminar premixed methane flames diluted with hot combustion products. Proc. Combust. Inst. **37**(4), 5095–5103 (2019). https://doi.org/10.1016/j.proci.2018.07.120

Knudsen, E., Kolla, H., Hawkes, E.R., Pitsch, H.: LES of a premixed jet flame DNS using a strained flamelet model. Combust. Flame **160**(12), 2911–2927 (2013). https://doi.org/10.1016/j.combustflame.2013.06.033

Kosaka, H., Zentgraf, F., Scholtissek, A., Bischoff, L., Häber, T., Suntz, R., Albert, B., Hasse, C., Dreizler, A.: Wall heat fluxes and CO formation/oxidation during laminar and turbulent side-wall quenching of methane and DME flames. Int. J. Heat Fluid Fl. **70**, 181–192 (2018). https://doi.org/10.1016/j.ijheatfluidflow.2018.01.009

Lai, J., Chakraborty, N.: Effects of Lewis number on head on quenching of turbulent premixed flames: a direct numerical simulation analysis. Flow Turbul. Combust. **96**(2), 279–308 (2016). https://doi.org/10.1007/s10494-015-9629-x

Lai, J., Klein, M., Chakraborty, N.: Direct numerical simulation of head-on quenching of statistically planar turbulent premixed methane-air flames using a detailed chemical mechanism. Flow Turbul. Combust. **101**(4), 1073–1091 (2018). https://doi.org/10.1007/s10494-018-9907-5

Mann, M., Jainski, C., Euler, M., Böhm, B., Dreizler, A.: Transient flame–wall interactions: Experimental analysis using spectroscopic temperature and CO concentration measurements. Combust. Flame **161**(9), 2371–2386 (2014). https://doi.org/10.1016/j.combustflame.2014.02.008

Norden, P.A.: Determination of quenching distance for carbon monoxide-air flames. J. Eng. Phys. Thermophys. **9**(1), 77–78 (1965). https://doi.org/10.1007/BF00831841

Palulli, R., Talei, M., Gordon, R.L.: Unsteady flame–wall interaction: Impact on CO emission and wall heat flux. Combust. Flame **207**, 406–416 (2019). https://doi.org/10.1016/j.combustflame.2019.06.012

Peters, N.: Turbulent Combustion. Cambridge Monographs on Mechanics. Cambridge University Press, Cambridge (2000)

Poinsot, T.J., Haworth, D.C., Bruneaux, G.: Direct simulation and modeling of flame-wall interaction for premixed turbulent combustion. Combust. Flame **95**(1), 118–132 (1993). https://doi.org/10.1016/0010-2180(93)90056-9

Popp, P., Baum, M.: Analysis of wall heat fluxes, reaction mechanisms, and unburnt hydrocarbons during the head-on quenching of a laminar methane flame. Combust. Flame **108**(3), 327–348 (1997). https://doi.org/10.1016/S0010-2180(96)00144-7

Smith, G.P., Golden, D.M., Frenklach, M., Moriarty, N.W., Eiteneer, B., Goldenberg, M., Bowman, C.T., Hanson, R.K., Song, S., Gardiner, W.C., Jr., Lissianski, V.V., Qin, Z.: Nd GRI3.0 (1999). https://www.me.berkeley.edu/gri_mech/.

Sotton, J., Boust, B., Labuda, S.A., Bellenoue, M.: Head-on quenching of transient laminar flame: heat flux and quenching distance measurements. Combust. Sci. Tech. **177**(7), 1305–1322 (2005). https://doi.org/10.1080/00102200590950485

Strassacker, C., Bykov, V., Maas, U.: REDIM reduced modeling of quenching at a cold wall including heterogeneous wall reactions. Int. J. Heat Fluid Fl. **69**, 185–193 (2018). https://doi.org/10.1016/j.ijheatfluidflow.2017.12.011

Strassacker, C., Bykov, V., Maas, U.: REDIM reduced modeling of flame quenching at a cold wall – The influence of detailed transport models and detailed mechanisms. Combust. Sci. Tech. **191**(2), 208–222 (2019). https://doi.org/10.1080/00102202.2018.1440216

Trisjono, P., Kleinheinz, K., Hawkes, E.R., Pitsch, H.: Modeling turbulence–chemistry interaction in lean premixed hydrogen flames with a strained flamelet model. Combust. Flame **174**, 194–207 (2016). https://doi.org/10.1016/j.combustflame.2016.07.008

van Oijen, J.A., de Goey, L.P.H.: Modelling of premixed counterflow flames using the flamelet-generated manifold method. Combust. Theor. Model. **6**(3), 463–478 (2002). https://doi.org/10.1088/1364-7830/6/3/305

Zhao, P., Wang, L., Chakraborty, N.: Analysis of the flame–wall interaction in premixed turbulent combustion. J. Fluid Mech. **848**, 193–218 (2018). https://doi.org/10.1017/jfm.2018.356

Zschutschke, A., Messig, D., Scholtissek, A., Hasse, C.: Universal Laminar Flame Solver (ULF). https://figshare.com/articles/ULF_code_pdf/5119855 (2017).